# A Well–Balanced Stable GRP Scheme for Shallow Water Equations for Adaptive Unstructured Triangular Meshes

**Feng Zhou[1], Guoxian Chen[2*], Sebastian Noelle[3] and Huai–Cheng Guo[4]**

**Bericht Nr. 364** **Mai 2013**

Key words: Shallow water equations, generalized Riemann problem, adaptive unstructured meshes, well-balanced scheme, hydrodynamic process.

AMS Subject Classifications: 65M08, 35L45, 35L65, 65M25, 65M50, 76L05

**Institut für Geometrie und Praktische Mathematik**
**RWTH Aachen**

**Templergraben 55, D–52056 Aachen (Germany)**

---

* Correspondence to: School of Mathematics and Statistics, Wuhan University, Wuhan, 430072, P.R. China. E-mail:gxchen.math@whu.edu.cn

Contract/grant sponsor: F. Zhou and H.C. Guo are partially supported by the National Water Science and Technology Research Project (No.2008ZX07102-006; 2012ZX07503-002) and the Shanghai Tongji Gao Tingyao Environmental Science & Technology Development Foundation. G. Chen is partially supported by the National Natural Science Foundation of China (No.11001211; No. 61179039). S. Noelle were supported by DFG Grant NO361/3-1 and No361/3-2.

1 Laboratory for Earth Surface Processes, College of Urban and Environmental Sciences, Peking University, Beijing, 100871, P.R. China.

2 School of Mathematics and Statistics, Wuhan University, Wuhan, 430072, P.R. China.

3 IGPM, RWTH Aachen, Templergraben 55, 52062, Aachen, Germany.

4 College of Environmental Sciences and Engineering, Peking University, Beijing, 100871, P.R. China.

# A well-balanced stable GRP scheme for shallow water equations for adaptive unstructured triangular meshes

Feng Zhou[1], Guoxian Chen[2*], Sebastian Noelle[3] and Huai-Cheng Guo[4]

[1]*Laboratory for Earth Surface Processes, College of Urban and Environmental Sciences, Peking University, Beijing, 100871, P.R. China.*
[2]*School of Mathematics and Statistics, Wuhan University, Wuhan, 430072, P.R. China.*
[3]*IGPM, RWTH Aachen, Templergraben 55, 52062, Aachen, Germany.*
[4]*College of Environmental Sciences and Engineering, Peking University, Beijing, 100871, P.R. China.*

SUMMARY

A well-balanced stable generalized Riemann problem (GRP) scheme under triangular meshes is proposed to solve shallow water equations (SWEs) involving irregular bottom topography, with the goal of the balance between flux gradients and bed slope source term, numerical stability, and high-performance computation. This scheme consists of two parts: an updated GRP evolution and adaptive mesh movement. The former is a second-order version Godunov method by evaluating the stability-preserving time-derivatives solutions along the exterior normal direction of the cell boundaries and by incorporating suitable central discretization of the bed source term. The latter is to move triangular meshes by iteratively solving Euler-Lagrange equations and remapping solutions on new meshes through geometrical conservative interpolations, which realizes still flat water property when the free surface is chosen as the interpolation variable. Three test cases were conducted to verify the performance of this updated scheme on the well-balanced stability-preserving property, predictive accuracy, spatial resolution, and computational efficiency. The results revealed two attractive features: (1) this scheme could preserve static flow by balancing bed slope and flux gradients through the application of unstructured triangular meshes with more stability through a modification of GRP time derivative calculation; (2) it could significantly improve the predictive accuracy and resolution of local features where gradients of flow variables are sharp, with a relatively lower computational cost.

KEY WORDS: Shallow water equations; generalized Riemann problem; adaptive unstructured meshes; well-balanced scheme; hydrodynamic process.

## 1. INDRODUCTION

Numerical scheme has become one of interesting topics for solving shallow water equations (SWEs) with shock-capturing capacity [1, 2, 3, 4, 3, 5, 6, 7, 8, 9, 10, 11, 12, 13, 14, 15, 16, 17]. To

*Correspondence to: School of Mathematics and Statistics, Wuhan University, Wuhan, 430072, P.R. China. E-mail:gxchen.math@whu.edu.cn

Contract/grant sponsor: F. Zhou and H.C. Guo are partially supported by the National Water Science and Technology Research Project (No.2008ZX07102-006; 2012ZX07503-002) and the Shanghai Tongji Gao Tingyao Environmental Science & Technology Development Foundation. G. Chen is partially supported by the National Natural Science Foundation of China (No.11001211; No. 61179039). S. Noelle were supported by DFG Grant NO361/3-1 and No361/3-2.

achieve high-order predictive accuracy, a generalized Riemann problem (GRP) scheme, originally designed for gas-dynamics [18, 19, 20], was developed as a second-order version Godunov scheme by evaluating the time-derivatives of variables on cell interface and incorporating the initial data MUSCL linear reconstruction for one dimensional case. This scheme has been widely applied in reaction flow [19], the motion of elastic string [21], open channel flow [22] and so on. Recently, a direct-Eulerian GRP method [15] was proposed under structured meshes for both Euler equations and shallow water equations with bottom topography [23, 24]. It adopted the main ingredient of Riemann invariants to decompose the nonlinear waves into a form of their simple super position, leading to resolving rarefaction waves analytically in a straight forward way. However, it is difficult to discretize complex domains using structured meshes; the GRP scheme needs to be extended to the application of unstructured triangular meshes. Moreover, when the time derivative of solution at cell interfaces solving by a linear system directly, the previous GRP scheme [15] becomes unstable for quasi-stationary states because that the water depth differences, small values for quasi-stationary states, between the two sides of cell interfaces are used as denominators and common factors for the linear system for the calculation of time derivatives. Therefore, it is essential to update the direct-Eulerian GRP method that applies unstructured meshes to provide stability-preserving solutions for SWEs with complex physical domain.

Recently, researchers have also demonstrated several important questions toward numerical schemes for SWEs, such as maintaining well-balanced property over complex topography [25, 26, 27], and positivity of water depth at the wet-dry interface [28, 29, 30, 30]. With regard to the first question, Russo [11] modified the Roe solver to preserve steady state [25]. Zhou et al. [14] developed a robust and well-balanced scheme based on a Godunov-type method and surface gradient method (SGM) for initial data reconstruction. Xu [31] proposed a well-balanced kinetic scheme for SWEs with a geometrical source term. Audusse et al. [1] designed a fast and stable well-balanced scheme by a hydrostatic reconstruction plus an additional correction of the source term, and it is also extended to two dimension case [2]. Noelle et al. [3] extended the scheme of [1] to arbitrary order of accuracy using numerical extrapolation. In one dimensional case, a high-order well-balanced finite volume WENO schemes for shallow water equation with moving water has been designed in [32]. To cope with the second question, Brufau et al. [28] proposed a modified approach to the wet-dry interface, including the normal velocity at the cell edge to achieve zero numerical errors. Audusse and Bristeau [2] as well as its cited references introduced a second-order local hydrostatic reconstruction that preserves positivity properties, which is simple to implement and entails none of the special treatment required by previous models. Therefore, it is necessary to explain whether GRP scheme to be updated for SWEs satisfies well-balanced positivity-preserving properties under unstructured meshes.

Another demand exists for additional researches on high-performance computation to capture discontinuous or nearly singular solutions efficiently in local features with higher spatial resolution but less unstructured meshes. Traditionally, fixed fine meshes are required to reproduce these small-scale features, which inevitably increase computational cost. In practice, it is desirable to apply adaptive meshes for improving the predictive accuracy of local features and maintaining high computational efficiency. Adaptive mesh methods can be applied to either refined or moving meshes. Adaptive refined meshes generate a desirable local high-resolution mesh obtained by repeatedly superimposing the grid with a grid in a higher subdivision level [33]. Unlike the AMR method [33],

the adaptive moving mesh (AMM) shift the fixed number of mesh points and redistribute the position of meshes to the desired regions [34, 35, 36, 36, 37, 38, 39]. For example, Tang and Tang [40] developed a general adaptive moving mesh method applying structured meshes, which can easily be applied to SWEs [41] with satisfaction of the stationary states property. Chen et al. [42] extended Tang and Tang's [40] method to two-dimensional compressible multi-material flows. Han et al. [43] presented a second-order accurate adaptive GRP scheme for one and two dimensional compressible fluid flows, Han et al. [44] also check the accuracy order of their scheme numerically. However, no work extends AMM method [42, 43, 41] to solve SWEs under unstructured meshes or proves its still flat water preserving property.

As an extension of previously works [42], this paper proposes a well-balanced stable GRP scheme for SWEs under adaptive-moving triangular meshes, with the goal of the balance between flux gradients and bed slope source term, stability-preserving time derivative calculation, and high-performance computation. The paper is organized as follows. Section 2 describes the general form of shallow water equations. Section 3 presents the updated GRP scheme under triangular meshes by modifying GRP time derivative evaluation and proving its well-balance property. Section 4 describes an adaptive moving mesh under triangular meshes with emphasis upon its proof of still flat water preserving property. Three benchmark cases are proposed in section 5 to verify the performance of our updated scheme in the numerical stability, predictive accuracy, spatial resolution, and computational efficiency.

## 2. SHALLOW WATER EQUATIONS

Ignoring Coriolis effects, viscous terms and surface stresses, two-dimensional depth-averaged SWEs, which approximate the depth and horizontal momentum of the flow , can be expressed as a hyperbolic conservative

$$\begin{cases} w_t + \nabla \cdot (h\mathbf{u}) = 0, \\ h\mathbf{u} + \nabla \cdot (h\mathbf{u} \otimes \mathbf{u}) + \nabla \left(\frac{1}{2} g h^2\right) = -gh\nabla b, \end{cases} \tag{1}$$

where $t$ denotes time, $\nabla = (\frac{\partial}{\partial x}, \frac{\partial}{\partial y})^\top$ is the vector of derivatives with respect to $x$ and $y$ coordinates, $h$ is the water depth, $\mathbf{u} = (u, v)$ is the flow velocity vector, $g$ is the gravitational acceleration constant, $b$ is the bed elevation, and $w = h + b$ is the free surface elevation.

In practice, an essential part for the SWEs (1) is required for steady state solutions in which the flux gradients should be exactly balanced by the source term. The general steady state solutions of the SWEs are given by

$$\begin{cases} \nabla \cdot (h\mathbf{u}) = 0, \\ \nabla p - \nabla \times \mathbf{u} \begin{pmatrix} v \\ u \end{pmatrix} = 0, \end{cases} \tag{2}$$

where is constant along streamlines and in irrotational areas, that is

$$p = \frac{|\mathbf{u}|^2}{2} + g(h + b) \tag{3}$$

Taking one-dimensional case for example, Noelle et al. [32] present a very high-order accurate, exactly well-balanced finite volume scheme for moving flow equilibria. Due to the complexity of the general equilibria in two-dimensional case, a still water steady state is applied to replace by

$$\mathbf{u} = 0 \quad \text{and} \quad h + b = C, \tag{4}$$

where $C$ is a constant, which plays a important role in the design of numerical schemes. Therefore, if the scheme can exactly preserve this property (4), it is well-balanced.

## 3. WELL-BALANCED STABLE GRP SCHEME FOR TRIANGULAR MESHES

In this section, the well-balanced property and stability-preserving time derivative would be exactly realized, leading to the update of previous GRP solver [15] for SWEs with bed topography under triangular meshes. Let $E_i$ denotes the $i$ th unstructured triangular element for the two-dimensional domain $\Omega_p \subset \mathbb{R}^2$ (Fig. 1). For the element $E_i$, we denote $\mathbf{x}_{ij} = (x_{ij}, y_{ij})$ its $j$th vertex, $E_{ij}$ its $j$th neighboring element, $l_{ij}$ its $j$th edge, $j = 1, 2, 3$, and $\mathbf{n}_{ij}$ its exterior normal vector on $l_{ij}$ from $E_i$ to $E_{ij}$. We denote by $\mathbf{U}_i^n$ as the integral average of flow variables $\mathbf{U} = (w, hu, hv)$ over $E_i$,

$$\mathbf{U}_i = \frac{1}{|E_i|} \int_{E_i} \mathbf{U}(\mathbf{x}, t) d\mathbf{x}. \tag{5}$$

We also replace the bottom function $b(\mathbf{x})$ with a continuous and piecewise linear approximation. Let $b(\mathbf{x}_{ij})$ denote the value of b at the vertex $\mathbf{x}_{ij}$, then a linear function $b_i(\mathbf{x})$ over the element $E_i$ is uniquely determined such that $b_i(\mathbf{x}_{ij}) = b(\mathbf{x}_{ij})$.

Figure 1. Schematic diagram of the unstructured triangular element. $E_i$ is the $i$th triangle of the triangulation. For the element $E_i$, we denote $\mathbf{x}_{ij} = (x_{ij}, y_{ij})$ is the $j$th vertex, $E_{ij}$ is the $j$th neighboring element, $l_{ij}$ is the $j$th edge, $j = 1, 2, 3$, and $\mathbf{n}_{ij}$ is the exterior normal vector on $l_{ij}$.

The integral form of Eq. (1) over $E_i$ is:

$$|E_i| \frac{\mathrm{d}\mathbf{U}_i}{\mathrm{d}t} = -\sum_{j=1}^{3} \int_{l_{ij}} \mathbf{F}_{\mathbf{n}_{ij}}(\mathbf{U}) \mathrm{d}s + \int_{E_i} \mathbf{S}(\mathbf{U}) \mathrm{d}\mathbf{x}, \tag{6}$$

in which $|E_i|$ denotes the triangle area, $ds$ is the edge length, $\mathbf{F}_{\mathbf{n}_{ij}}(\mathbf{U})$ represents the flux along the direction $\mathbf{n}_{ij} = (\mathbf{n}_{ij}^x, \mathbf{n}_{ij}^y)^{\mathrm{T}}$. $\mathbf{S}(\mathbf{U}) = (0, -ghb_x, -ghb_y)^T$ denotes the source term. All the integrations in Eq. (6) can be approximated using the central scheme. The central difference method can be used to update the flow variables to a new time step, as follows:

$$\mathbf{U}_i^{n+1} = \mathbf{U}_i^n - \frac{\Delta t}{|E_i|} \sum_{j=1}^{3} \mathbf{F}_{\mathbf{n}_{ij}}(\mathbf{U})_{ij}^{n+1/2} |l_{ij}| + \Delta t \mathbf{S}(\mathbf{U})_i^{n+1/2} \tag{7}$$

where the superscript $n$ denotes the time level, $\Delta t$ is the time step, $|l_{ij}|$ denotes the length of the edge $l_{ij}$, $\mathbf{F}_{\mathbf{n}_{ij}}(\mathbf{U})_{ij}^{n+1/2}$ and $\mathbf{S}(\mathbf{U})_i^{n+1/2}$ are the approximate values of flux $\mathbf{F}_{\mathbf{n}_{ij}}(\mathbf{U})$ and bed slope

source term $\mathbf{S}(\mathbf{U})$ respectively, which are evaluated at mid-time $t_n + \Delta t/2$ and the cell center $\mathbf{x}_{l_{ij}}$ of edge $l_{ij}$ respectively:

$$\mathbf{F}_{\mathbf{n}_{ij}}(\mathbf{U})_{ij}^{n+1/2} = \mathbf{F}_{\mathbf{n}_{ij}}(\mathbf{U}_{ij}^{n+1/2}), \tag{8}$$

and

$$\mathbf{S}(\mathbf{U})_i^{n+1/2} = -\frac{1}{|E_i|}\sum_{j=1}^{3}\begin{pmatrix} 0 \\ g\frac{h_{ij}^{n+1/2}+\bar{h}_i^{n+1/2}}{2}(b_{ij}-b_i)\,|l_{ij}|\mathbf{n}_{ij} \end{pmatrix}, \tag{9}$$

where $\mathbf{U}_{ij}^{n+1/2}$ is evaluated by the Taylor expansion up to first order in time as

$$\mathbf{U}_{ij}^{n+1/2} = \mathbf{U}(\mathbf{x}_{l_{ij}}, t_n + \frac{\Delta t}{2}) \;\approx\; \mathbf{U}_{ij}^{n} + \frac{\Delta t}{2}\left(\frac{\partial \mathbf{U}}{\partial t}\right)_{ij}^{n}, \tag{10}$$

and

$$\bar{h}_i^{n+1/2} = \frac{1}{3}\sum_{j=1}^{3} h_{ij}^{n+1/2}, \tag{11}$$

Estimations of $\mathbf{F}_{\mathbf{n}_{ij}}(\mathbf{U})_{ij}^{n+1/2}$ and $\mathbf{S}(\mathbf{U})_i^{n+1/2}$ require the computations of $\mathbf{U}_{ij}^n$ and $(\frac{\partial \mathbf{U}}{\partial t})_{ij}^n$. After the second order initial data reconstruction for spatial resolution, $\mathbf{U}_{ij}^n$ are calculated from the associated Riemann problem for the homogeneous conservation. Unlike the approach of previous work [15], the solver of time derivative $(\frac{\partial \mathbf{U}}{\partial t})_{ij}^n$ needs to be more stable for the quasi-stationary states. After obtaining $\mathbf{F}_{\mathbf{n}_{ij}}(\mathbf{U})_{ij}^{n+1/2}$ and $\mathbf{S}(\mathbf{U})_i^{n+1/2}$, the flow variables $\mathbf{U}_i^{n+1}$ can be computed using Eq. (7). The well-balanced property will also be exactly preserved.

### *3.1. Initial data reconstruction*

To obtain a second-order accurate approximation of the initial data, we reconstruct a piecewise linear function for primitive variable vector $\mathbf{W} = (h + b, u, v)^\top$ over element $E_i$,

$$\mathbf{W}(\mathbf{x}) = \mathbf{W}_i^n + \varphi_i \nabla \mathbf{W}_i^n \cdot \mathbf{r}, \tag{12}$$

where $\nabla \mathbf{W}_i^n$ is the gradient of $\mathbf{W}$ obtained using Green's theorem from the average values over three adjacent elements. $\varphi \in [0, 1]$ is a chosen limiter function; if $\varphi_i$ is equal to zero, then the flow variables are approximated as a piecewise constant function and spatial accuracy is only first-order. If $\varphi_i$ is equal to 1, spatial accuracy is second-order accurate. A slope limiter is required to control instability and to prevent oscillation around the vicinity of the shock; $\varphi$ can be derived using an upwind type limiter as follows:

$$\varphi_i = \begin{cases} \min(1, \frac{\mathbf{W}_j^{\max}-\mathbf{W}_i}{\mathbf{W}_{ij}^L-\mathbf{W}_i}), & \text{if } \mathbf{W}_{ij}^L - \mathbf{W}_i > 0, \\ \min(1, \frac{\mathbf{W}_j^{\min}-\mathbf{W}_i}{\mathbf{W}_{ij}^L-\mathbf{W}_i}), & \text{if } \mathbf{W}_{ij}^L - \mathbf{W}_i < 0, \\ 1, & \text{if } \mathbf{W}_{ij}^L - \mathbf{W}_i = 0. \end{cases} \tag{13}$$

### *3.2. Stability-preserving GRP time derivative calculation*

For the convenience of writing without reading confusion, we still use x and y instead of the coordinate variables along the local normal and tangential direction of edge $l_{ij}$, and use u and

v instead of the normal velocity $u\mathbf{n}_{ij}^x + v\mathbf{n}_{ij}^y$ and tangential velocity $-u\mathbf{n}_{ij}^y + v\mathbf{n}_{ij}^x$, respectively. Because of the rotational invariance, the governing equations along the exterior normal direction of edge $l_{ij}$ take this form as follows

$$\frac{\partial}{\partial t}\begin{pmatrix} w \\ hu \\ hv \end{pmatrix} + \frac{\partial}{\partial x}\begin{pmatrix} hu \\ hu^2 + \frac{1}{2}gh^2 \\ hv \end{pmatrix} = \begin{pmatrix} 0 \\ -ghb_x \\ 0 \end{pmatrix}, \tag{14}$$

the corresponding initial data given by (12) is

$$\mathbf{W}(x, t=0) = \begin{cases} \mathbf{W}_- + x \cdot \delta\mathbf{W}_-, & x < 0, \\ \mathbf{W}_+ + x \cdot \delta\mathbf{W}_+, & x > 0. \end{cases} \tag{15}$$

where $\mathbf{W}_-$ and $\mathbf{W}_+$ denote the left and right limit values at point $\mathbf{x}_{l_{ij}}$, $\delta\mathbf{W}_-$ and $\delta\mathbf{W}_+$ are the corresponding left and right limit slop values along exterior normal direction at point $\mathbf{x}_{l_{ij}}$.

After the calculation of $\mathbf{U}_0 = \mathrm{R}(0; \mathbf{W}_-, \mathbf{W}_+)$ using the homogeneous Riemann problem without the effect of the bed slop source term, the time derivative $\frac{\partial \mathbf{U}}{\partial t}_0$ is obtained by direct GRP method including the influence of the initial and bed slops in (15). The main point is to obtain $\frac{\partial h}{\partial t}_0$ and $\frac{\partial u}{\partial t}_0$ by solving a linear system including two variables:

$$\begin{cases} a_-^1 \left(\frac{\partial h}{\partial t}\right)_0 + a_-^2 \left(\frac{\partial u}{\partial t}\right)_0 = d_-, \\ a_+^1 \left(\frac{\partial h}{\partial t}\right)_0 + a_+^2 \left(\frac{\partial u}{\partial t}\right)_0 = d_+, \end{cases} \tag{16}$$

where $a_-^1$, $a_-^2$ and $d_-$ ($a_+^1$, $a_+^2$ and $d_+$) are constants that depend on $\mathbf{W}_-$, $\delta\mathbf{W}_-$, $b$ and $\delta b_-$ ( $\mathbf{W}_+$, $\delta\mathbf{W}_+$, $b$, and $\delta b_+$) and the associate Riemann solver $\mathbf{W}_* = \mathrm{R}(0; \mathbf{W}_-, \mathbf{W}_+)$. To shorten the length of this paper, the deduce details of GRP solver are not appeared in this paper but could be found in the second author's previous work [15]. Here we only give the expression for a typical case, e.g., the left rarefaction wave resolution and right shock wave resolution, because the other cases could be addressed similarly. And the linear system for the GRP time derivative calculation will be modified to become more stable. The change from physical coordinates to characteristic coordinates plays important role for the calculation of the left rarefaction wave resolution. According to [15], the coefficients $a_-^1$, $a_-^2$ and $d_-$ takes this values,

$$\begin{aligned} (a_-, b_-) &= (\mu_* - \lambda_*)\nabla_{(h,u)} s_* \cdot A_*^{-1}, \\ d_- &= \left(\frac{\partial t(0,\beta_*)}{\partial \alpha}\right)^{-1} \frac{\partial s(0,\beta_*)}{\partial \alpha} - \lambda_* \nabla_{(h,u)} s_* \cdot A_*^{-1} \cdot \prod(0), \end{aligned} \tag{17}$$

where $\beta$ and $\alpha$ are the first and last characteristic coordinates corresponding the eigenvalues,

$$\lambda = u - \sqrt{gh} \quad \text{and} \quad \mu = u + \sqrt{gh}. \tag{18}$$

Other variables are

$$s = u + 2\sqrt{gh}, \quad \prod = (0, -gb'(x))^T \quad \text{and} \quad A = \begin{pmatrix} u & h \\ g & u \end{pmatrix}. \tag{19}$$

The Rankine-Hugoniot jump relation is the key for the right shock resolution. The coefficients $a_+^1$, $a_+^2$ and $d_+$ were given by

$$\begin{aligned}(a_+, b_+) &= \nabla_{(h,u)} G(h_*, u_*) \cdot (A(h_*, u_*) - \gamma_* I) A^{-1}(h_*, u_*), \\ d_+ &= \nabla_{(h_+,u_+)} G(h_*, u_*) \cdot (A(h_+, u_+) - \gamma_* I) \cdot (\delta h_+, \delta u_+) \\ &\quad -\gamma_* \nabla_{(h,u)} G(h_*, u_*) \cdot A^{-1}(h_*, u_*) \prod(0) - \nabla_{(h+,u+)} G \cdot \prod(0),\end{aligned} \tag{20}$$

where

$$G(h, u, h_+, u_+) = h h_+ (u - u_+)^2 - \frac{g}{2}(h + h_+)(h - h_+)^2 \tag{21}$$

and it gradients with respect to $(h, u)$ and $(h_+, u_+)$ are

$$\begin{aligned}\nabla_{(h,u)} G &= (h - h_+) \left( -\tfrac{g}{2h}(2h^2 + h_+^2 + h h_+), 2h h_+ \tfrac{u - u_+}{h - h_+} \right), \\ \nabla_{(h_+,u_+)} G &= (h_+ - h) \left( -\tfrac{g}{2h_+}(2h_+^2 + h^2 + h h_+), 2h h_+ \tfrac{u - u_+}{h - h_+} \right),\end{aligned} \tag{22}$$

$\gamma_* = \gamma(0)$ is the initial shock speed. Notice that the difference between $h_*$ and $h_+$ will be the denominator and the factor in the coefficients $a_+^1$, $a_+^2$ and $d_+$ when substitute the above two gradient formulas into (20). While the depth difference becomes small for the quasi-stationary states and even equals zero for stationary states. The small values will make the linear system (16) degradation and even singular for stationary states. This will make the calculation of time derivative unstable. Therefore, the coefficients in the linear system (20) are modified through two steps. First, the coefficient $(u_* - u_+)/(h_* - h_+)$ is replaced as

$$\frac{u_* - u_+}{h_* - h_+} = \sqrt{\frac{g(h_* + h_+)}{2 h_* h_+}}, \tag{23}$$

using Rankine-Hugoniot condition $G(h_*, u_*, h_+, u_+) = 0$; second, the common factor $h_* - h_+$ is removed from both sides in the second equation of (16). Finally, the calculation of linear system will become more stable where no coefficients become singular.

### *3.3. Well-balanced property*

We also provide an algebraic proof to explain the updated GRP scheme applying unstructured triangular meshes satisfies the well-balanced property, i.e. $h_i^n + b_i^n = C$, $\mathbf{u}_i^n = 0$ implies $h_i^{n+1} + b_i^{n+1} = C$, $\mathbf{u}_i^{n+1} = 0$ for all $i$. From the reconstruction (12), the local GRP initial data (15) in local coordinates on every edge satisfy

$$h_- + b = h_+ + b = C, \quad \mathbf{u}_- = \mathbf{u}_+ = 0, \tag{24}$$

and

$$\delta h_- + \delta b_- = \delta h_+ + \delta b_+ = 0, \quad \delta \mathbf{u}_- = \delta \mathbf{u}_+ = 0. \tag{25}$$

The associate Riemann solver $\mathrm{R}(0; \mathbf{W}_-, \mathbf{W}_+)$ implies that

$$h_0 + b = C \quad \text{and} \quad \mathbf{u}_0 = 0. \tag{26}$$

Applying the above stable GRP method where the linear system are modified, the time derivative of primitive variables are

$$\left(\frac{\partial h}{\partial t}\right)_0 = \left(\frac{\partial \mathbf{u}}{\partial t}\right)_0 = 0 \tag{27}$$

resulting in the predicted values on every edge as

$$h_{ij}^{n+1/2} + b_{ij} = C \quad \text{and} \quad \mathbf{u}_{ij}^{n+1/2} = 0. \tag{28}$$

By substituting the above values for the numerical fluxes (8) and bed slop source terms (9), the mass flux becomes zero on every edge. Using the first equation of (7), the updated free surface is

$$w_i^{n+1} = h_i^{n+1} + b_i = C. \tag{29}$$

The update of the momentum using the second and third components of vector equations (7) is given by

$$\frac{|E_i|}{\Delta t}((h\mathbf{u})_i^{n+1} - (h\mathbf{u})_i^n) = -\sum_{j=1}^{3} \frac{g\left(h_{ij}^{n+1/2}\right)^2}{2} |l_{ij}|\mathbf{n}_{ij} - \sum_{j=1}^{3} g\frac{h_{ij}^{n+1/2} + \bar{h}_i^{n+1/2}}{2}(b_{ij} - b_i)\,|l_{ij}|\mathbf{n}_{ij}. \tag{30}$$

Merging the common factors, the above formula becomes,

$$\frac{|E_i|}{\Delta t}((h\mathbf{u})_i^{n+1} - (h\mathbf{u})_i^n) = -\sum_{j=1}^{3} \left[\frac{g\left(h_{ij}^{n+1/2}\right)^2}{2} + g\frac{h_{ij}^{n+1/2} + \bar{h}_i^{n+1/2}}{2}(b_{ij} - b_i)\right] |l_{ij}|\mathbf{n}_{ij}. \tag{31}$$

Adding the following expression into the right hand side of the above expression,

$$\sum_{j=1}^{3} \frac{g\left(\bar{h}_i^{n+1/2}\right)^2}{2} |l_{ij}|\mathbf{n}_{ij} = \frac{g\left(\bar{h}_i^{n+1/2}\right)^2}{2} \sum_{j=1}^{3} |l_{ij}|\mathbf{n}_{ij} = 0, \tag{32}$$

where $\bar{h}_i^{n+1/2} = \frac{1}{3}\sum_{k=1}^{3} h_{ik}^{n+1/2}$, we get the update formula for momentum,

$$\frac{|E_i|}{\Delta t}((h\mathbf{u})_i^{n+1} - (h\mathbf{u})_i^n) = -\sum_{j=1}^{3} \left[\frac{g\left(h_{ij}^{n+1/2}\right)^2}{2} - \frac{g\left(\bar{h}_i^{n+1/2}\right)^2}{2} + g\frac{h_{ij}^{n+1/2} + \bar{h}_i^{n+1/2}}{2}(b_{ij} - b_i)\right] |l_{ij}|\mathbf{n}_{ij}. \tag{33}$$

After some simple calculation, we have

$$\frac{|E_i|}{\Delta t}((h\mathbf{u})_i^{n+1} - (h\mathbf{u})_i^n) = -\sum_{j=1}^{3} g\frac{h_{ij}^{n+1/2} + \bar{h}_i^{n+1/2}}{2}\left((h_{ij}^{n+1/2} + b_{ij}) - (\bar{h}_i^{n+1/2} + b_i)\right) |l_{ij}|\mathbf{n}_{ij}. \tag{34}$$

Because of Eq. (28), we know that

$$\bar{h}_i^{n+1/2} + b_i = \frac{1}{3}\sum_{k=1}^{3}(h_{ik}^{n+1/2} + b_{ik}) = \frac{1}{3}\sum_{k=1}^{3} C = C, \tag{35}$$

therefore

$$\frac{|E_i|}{\Delta t}((h\mathbf{u})_i^{n+1} - (h\mathbf{u})_i^n) = 0. \tag{36}$$

The updated momentums on the new time level then satisfy

$$(h\mathbf{u})_i^{n+1} = 0, \tag{37}$$

then the updated velocity vector will be zero,

$$\mathbf{u}_i^{n+1} = 0, \tag{38}$$

The formulas (29) and (38) indicate that the updated GRP scheme can exactly preserve the well-balanced property under unstructured triangular meshes.

## 4. ADAPTIVE MOVING MESH METHOD FOR UNSTRUCTURED TRIANGULAR CELLS

Extending on a previously-developed method [40, 42], we adopt an adaptive moving mesh method for SWEs under triangular meshes, in which still flat water property will also be proved as preserved explicitly while triangular meshes moving. The method involves two steps: mesh movement and conservative interpolation. Before explaining these steps in the following sections, let $\Omega_l$ denote the logical domain at Cartesian coordinates $\xi = (\xi, \eta)$. The initial partition $\mathcal{T}_l$ of $\Omega_l$ share the same data structure with partition $\mathcal{T}$ of the physical domain $\Omega_p$ of the flow variables.

### *4.1. Mesh movement based on the variational principle*

To adapt the meshes to the desired positions, it is necessary to solve mesh partial differential equations (PDEs), which define a mapping function from the logical domain to the physical domain as $\mathbf{x} = \mathbf{x}(\xi)$, where $\xi \in \Omega_l$ is based on the variational principle. To minimize an energy functional equations [40, 42] , mesh PDEs can be transferred to Euler-Lagrange equations, as follows:

$$\tilde{\nabla} \cdot (\omega \tilde{\nabla} \mathbf{x}) = 0 \tag{39}$$

where $\tilde{\nabla} = \nabla_\xi = (\frac{\partial}{\partial \xi}, \frac{\partial}{\partial \eta})$ are gradient operators with respect to the logical coordinates $\xi$. $\omega$ is the monitor function related to the solution and the gradient of the solution, that is; $\omega = \omega(\mathbf{U}_i^{[\nu]}, \tilde{\nabla}\mathbf{U}_i^{[\nu]})$. $[\nu]$ is the iteration step. First, consider mesh movement in the inner region. The integral form of Eq. (39) over the dual cell in logical domain results in a finite volume discrete system as follows:

$$\sum_{j=1}^{N(i)} \omega_{ij} \left|\hat{l}_{ij}\right| \frac{\mathbf{x}_{ij} - \mathbf{x}_i}{|\xi_{ij}\xi_i|} = 0 \tag{40}$$

Generally, the above equation is a nonlinear system because it depends on $\omega_{ij} = \omega(\mathbf{U}(\xi_{ij}))$. To simplify the calculation, this system is linearized and solved using a relaxed Jacobi iteration,

resulting in:

$$\begin{cases} \hat{\mathbf{x}}_i = \sum_{j=1}^{N(i)} \varpi_{ij}\mathbf{x}_{ij}^{[\nu]} / \sum_{j=1}^{N(i)} \mathbf{x}_{ij}^{[\nu]} \\ \\ \mathbf{x}_i^{[\nu+1]} = \mu_i \hat{\mathbf{x}}_\mathbf{i} + (\mathbf{1} - \mu_\mathbf{i})\mathbf{x}_\mathbf{ij}^{[\nu]} \end{cases} \qquad \nu = 0, 1, \cdots \tag{41}$$

in which

$$\varpi_{ij} = \frac{\Delta\tau}{|V_i|}\omega_{ij}\left|\hat{l}_{ij}\right| / |\xi_{ij}\xi_i|, \qquad \mu_i = \max\left\{\sum_{j=1}^{N(i)} \varpi_{ij}, \sigma\right\} \tag{42}$$

where $\mathbf{x}_{ij}^{[\nu]}$ is an adjacent node of $\hat{\mathbf{x}}_i$, $N(i)$ was the number of all adjacent nodes; $\Delta\tau$ and control the quality of the cells, determined in this study to be $\Delta\tau = 0.5$ and $\sigma = 0.3$. Because the goal of mesh movement is to adjust the cell positions to enhance the resolution of modified SWEs, it is not necessary to solve mesh PDEs completely. $\left|\mathbf{x}_i^{[\nu+1]} - \mathbf{x}_i^{[\nu]}\right| \leq 10^{-6}$ or $\nu = 5$ were chosen as the criterion to end the iterations. Additionally, the boundary mesh points should be redistributed simultaneously along with inner mesh movement, because discontinuity in the regions of interest could interact with the boundaries. A detailed explanation of this boundary mesh movement can be found in Chen et al. [42].

Figure 2. Schematic diagram of triangular mesh movement from $E_i^{[\nu]}$ to $E_i^{[\nu+1]}$. Note: $\mathbf{x}_{i1}^{[\nu]}$, $\mathbf{x}_{i2}^{[\nu]}$ and $\mathbf{x}_{i3}^{[\nu]}$ are the nodes in $E_i^{[\nu]}$ while $\mathbf{x}_{i1}^{[\nu+1]}$, $\mathbf{x}_{i2}^{[\nu+1]}$ and $\mathbf{x}_{i3}^{[\nu+1]}$ are the nodes in $E_i^{[\nu+1]}$ ; $D_{ij}$ is the region scanned by the edge $l_{ij}^{[\nu]}$.

### *4.2. Geometrical conservative interpolation*

After obtaining the new cell position $\mathbf{x}_{ij}^{[\nu+1]}$, the average value $\mathbf{U}_i^{[\nu+1]}$ on the new meshes can be obtained using conservative interpolation based on $\mathbf{U}_i^{[\nu]}$ defined for the old meshes [40, 45, 42].

Geometrical interpolation updates the conservative variables by summing the total mass over the old mesh, and the mass fluxes over the scanned region $D_{ij}$ of edge $l_{ij}$:

$$\begin{cases} |E_i^{[\nu+1]}|\mathbf{U}_i^{[\nu+1]} = |E_i^{[\nu]}|\mathbf{U}_i^{[\nu]} + \sum_{j=1}^{3} \hat{\mathbf{F}}(\mathbf{U}_{ij}^L, \mathbf{U}_{ij}^R) \\ \\ \hat{\mathbf{F}}(\mathbf{U}_{ij}^L, \mathbf{U}_{ij}^R) = \max\{|D_{ij}|, 0\}\mathbf{U}_{ij}^L + \min\{|D_{ij}|, 0\}\mathbf{U}_{ij}^R \end{cases} \tag{43}$$

where mass flux $\hat{\mathbf{F}}(\mathbf{U}_{ij}^L, \mathbf{U}_{ij}^R)$ is the approximate integration of $\mathbf{U}$ over domain $D_{ij}$, and $\mathbf{U}_{ij}^L$ and $\mathbf{U}_{ij}^R$ are the reconstructed values from $\mathbf{U}_i^{[\nu]}$ using Eq. (12). To obtain the mass flux, it is essential to calculate the signed area $|D_{ij}|$ such that it is positive if $l_{ij}$ scans to the right, and vice versa. This can easily be computed for triangular mesh; for example, $|D_{i0}|$ can be calculated by:

$$|D_{i0}| = \frac{1}{2}\left[(x_{i3}^{[\nu+1]} - x_{i2}^{[\nu]})(y_{i3}^{[\nu]} - y_{i2}^{[\nu+1]}) - (y_{i3}^{[\nu+1]} - y_{i2}^{[\nu]})(x_{i3}^{[\nu]} - x_{i2}^{[\nu+1]})\right] \tag{44}$$

Mass flux calculation is essentially an upwind method because it is greater than zero if an edge moves away from the element, and vice versa. Certainly, mass flux satisfies $\hat{\mathbf{F}}(\mathbf{U}_{ij}^L, \mathbf{U}_{ij}^R) = -\hat{\mathbf{F}}(\mathbf{U}_{ij}^R, \mathbf{U}_{ij}^L)$, resulting in the conservative property of flow variables within the interpolation step.

### *4.3. Still flat water preserving property*

Similar with well-balanced property in the last section, we consider the still flat water preserving property while the meshes is moving, i.e. $h_i^{[\nu]} + b_i^{[\nu]} = C$ and $\mathbf{u}_i^{[\nu]} = 0$ implies $h_i^{[\nu+1]} + b_i^{[\nu+1]} = C$ and $\mathbf{u}_i^{[\nu+1]} = 0$ for all $i$. After initial data reconstruction (12) , we obtained $h_{ij}^L + b_{ij} = h_{ij}^R + b_{ij} = C$ and $\mathbf{u}_{ij}^L = \mathbf{u}_{ij}^R = 0$. Flux $\hat{\mathbf{F}}(\mathbf{U}_{ij}^L, \mathbf{U}_{ij}^R)$ was equal to $|D_{ij}|(C, 0, 0)^{\mathbf{T}}$, so Eq. (43) can be updated as follows:

$$|E_i^{[\nu+1]}|\mathbf{U}_i^{[\nu+1]} = \left(|E_i^{[\nu]}| + \sum_{j=1}^{3} |D_{ij}|\right) \mathbf{U}_i^{[\nu]}. \tag{45}$$

According to the calculation of signed area $|D_{ij}|$, we have:

$$|E_i^{[\nu+1]}| = |E_i^{[\nu]}| + \sum_{j=1}^{3} |D_{ij}|, \tag{46}$$

Substitute the above formula into (45), the updated $\mathbf{U}_i^{[\nu+1]}$ is then equal to $\mathbf{U}_i^{[\nu]}$, resulting in $h_i^{[\nu+1]} + b_i^{[\nu+1]} = C$ and $\mathbf{u}_i^{[\nu+1]} = 0$, which indicates that the proposed adaptive moving meshes can preserve the still flat water.

## 5. SOLUTION ALGORITHM

To facilitate use of the well-balanced stable GRP scheme, source code was developed in FORTRAN language with double precision following the general solution algorithm:

**Step 1** : Input the initial data. Give the initial mesh $\{x_i^0\}$ and $\{\xi_i^0\}$ for both the physical domain and logical domain , respectively. Calculate the average value $\mathbf{U}_i^n$ for the conservative variable $\mathbf{U}$ over every physical control volume; let $n = 0$.

**Step 2** : Adaptive moving of triangular meshes. Let$\nu := 0$, $\mathbf{x}_i^{[0]} := \mathbf{x}_i^n$, and $\mathbf{U}_i^{[0]} := \mathbf{U}_i^n$.

**A1** . Adjust the cells $\mathbf{x}^{[\nu]}$ to the new position $\mathbf{x}^{[\nu+1]}$ by solving the mesh movement equations using (41).

**A2** . Update the conservative flow variables $\mathbf{U}_i^{[\nu+1]}$ over the new meshes according to (43).

**A3** . If $\left|\mathbf{x}_i^{[\nu+1]} - \mathbf{x}_i^{[\nu]}\right|$ is not greater than $10^{-6}$ or $\nu = 5$, then set $\mathbf{x}_i^{n+1} := \mathbf{x}_i^{[\nu+1]}$, $\mathbf{U}_i^n := \mathbf{U}_i^{[\nu+1]}$ and go to step 3, otherwise set $\nu := \nu + 1$ and progress to B1.

**Step 3** : Solve the SWEs over the new meshes.

**B1** . Solve the SWEs for the fixed meshes $\{\mathbf{x}_i^{n+1}\}$ using the stable GRP finite volume method given in Section 3.2, to achieve the numerical solution $\mathbf{U}_i^{n+1}$ at the time $t = t_{n+1}$.

**B2** . If $t_{n+1} < TSTOP$, where TSTOP is simulation of time, then let $n := n + 1$ and go back to step 2. Otherwise, export the solution $\mathbf{x}_i^{n+1}$ and $\mathbf{U}_i^{n+1}$ and exit the program.

## 6. RESULTS AND DISCUSSION

A series of model tests were performed to verify the well-balanced stable GRP scheme under adaptive triangular meshes outlined above; model predictions were compared with alternative numerical solutions in terms of the well-balanced stability-preserving property and computational features. Three test cases were performed: (i) a partial dam-break flow problem over flat bed, (ii)still water flow over a smooth bed, (iii)still water with a small perturbation over a smooth bed. For all tests, $g$ is constant at $9.8m/s^2$, respectively. Computations for the numerical examples presented below were performed on an Intel® Core™ i5 CPU M480 @ 2.67GHz with 3 GB RAM. The initial triangular meshes were generated by EASYMESH (http://www-dinma.univ.trieste.it/nirftc/research/easymesh/). Because choosing a monitor function was not the main goal of this study, we applied the traditional method of an arclength-type monitor (AL-monitor), such as $\omega_i = \sqrt{1+\alpha\tilde{\omega}_i^2(\beta, h+b)}$, where $\alpha$ and $\beta \in (0,1]$ are problem-dependent nonnegative constants, $\tilde{\omega}_i$ represents the physical variables; that is, $\tilde{\omega}_i(\beta, h+b) =: \min\left\{1, |\nabla_\xi(h+b)|_i / \beta \max_i |\nabla_\xi(h+b)|_i\right\}$, Here, $\beta$ is constant at 0.25 [42].

### 6.1. *Partial dam-break flow over flat bottom*

We used a classical two-dimensional partial dam-break flow case to validate the shock-capturing and computational efficiency of our proposed numerical scheme for flat bed. This test case has been widely used in the literature [46, 47, 48], however, no analytical solution is available. The model domain was composed of a 200m $\times$ 200m basin over a flat, fixed, and frictionless bed. Water depths were 10m and 5m on the left and right sides of the dam wall, respectively; Fig.3 A lists size parameters. The left and right sides of the computational domain were infiltrative while other boundaries were reflex.

In the current study, we used $\alpha = 10$. Model domains were divided into $7,409$ and $29,217$ triangular cells for coarse and fine meshes, respectively, and mesh redistribution was based on coarse triangular cells. Table I lists the other parameters of the triangular meshes and CPU times for the GRP scheme under fixed coarse meshes, fixed fine meshes, and adaptive moving meshes. At $t = 0$, a breach with a width of 75m centered at $y = 132.5$m formed instantly. After the dam broke, a shock wave formed and propagated downstream, while a depression wave spread upstream. Fig.3 presents the predicted free surface elevation and the associated mesh at $t = 7.2$; the results support previously-developed models [46, 47, 48]. However, numerical solutions applying adaptive moving meshes were distinct from those of coarse and fixed meshes, even when they had the same number of cells. Unlike when coarse fixed mesh was applied in the initial state (Figs.3A and 3D), the adaptive moving mesh method efficiently clustered mesh points at $t = 7.2$ to relatively local regions where gradients in free surface elevation varied significantly (Fig.3C), including two non-convex regions and right-moving shock waves. Mesh points were sparsely redistributed when gradients of free surface elevation were relatively lower. Therefore, the predictive accuracy and spatial resolution were relatively higher in non-convex regions and right-moving shock waves Fig.3F

Although the fixed fine meshes applied four times of cells (29,217, Fig.3B), its predictive accuracy and spatial resolution were inferior to those of the adaptive moving meshes method (Fig.3E). Additionally, the CPU time required at $t = 7.2$ was 251s for the GRP scheme using fixed fine mesh, consuming 206 more CPU time than adaptive moving meshes. Figure 5 shows solutions

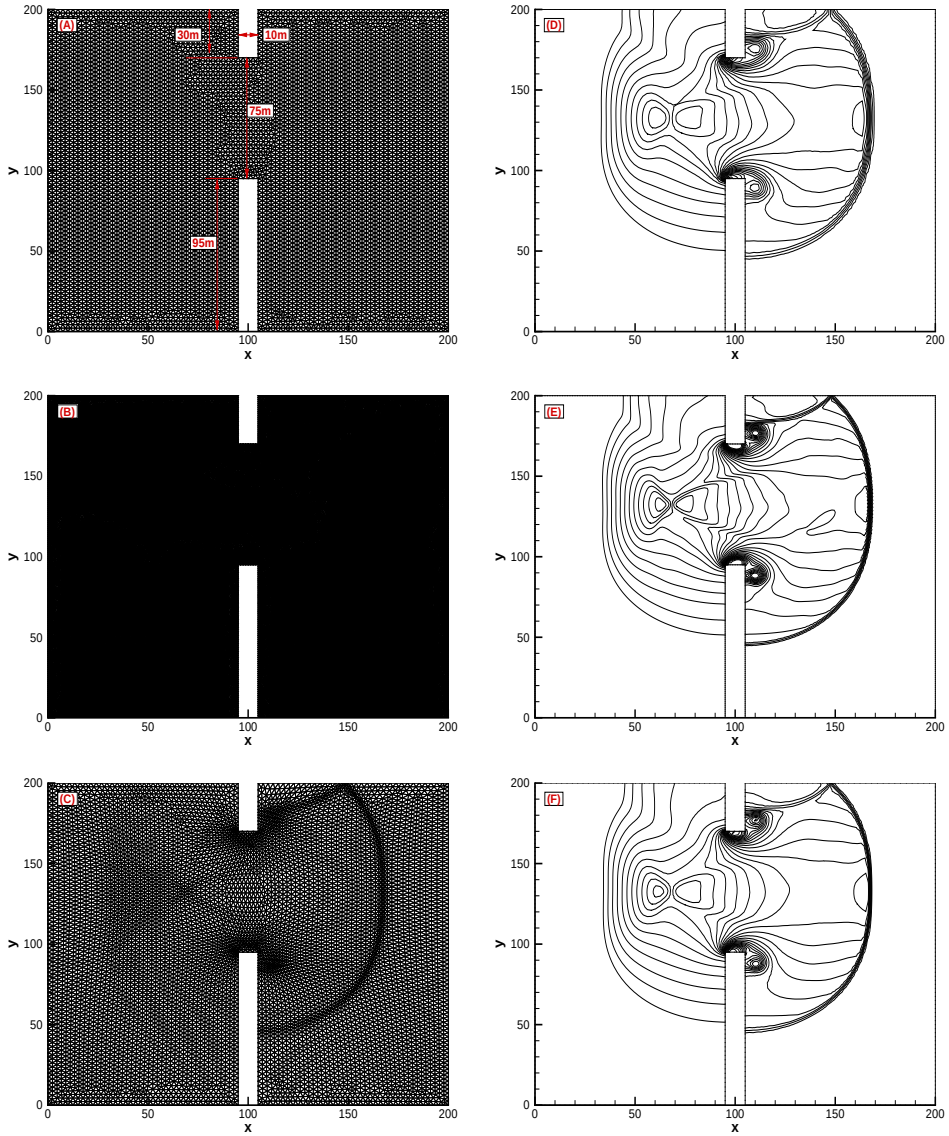


Figure 3. Numerical solutions and the associated meshes of adaptive GRP scheme for a partial dam-break flow problem at $t = 7.2$. Contour lines of free surface elevation for fixed coarse, fixed fine, and adaptive moving meshes were illustrated.

| Algorithm | # cells | # nodes | max/min $\|l_{ij}\|$ | max/min $\|E_i\|$ | CPU time(s) |
|---|---|---|---|---|---|
| Fixed coarse meshes | 7409 | 14396 | 3.02/1.84 | 3.55/1.70 | 30 |
| Fixed fine meshes | 29217 | 57592 | 1.60/0.71 | 0.94/0.27 | 251 |
| Adaptive moving meshes | 7409 | 14396 | 4.71/0.60 | 5.14/0.36 | 122 |

Table I. Mesh parameters and CPU time of a partial dam-breach flow problem computed under fixed coarse, fixed fine, and adaptive moving meshes. The simulation time is 7.2. $|l_{ij}|$ and $|E_i|$ are the edge length and triangle area, respectively.

at the same times along the line $y = 132.5$m. Mean, range, and standard deviation of the absolute value of the discrepancy between the numerical solutions of fixed fine and adaptive moving meshes were $0.015$, $0.165$, and $0.016$, respectively, while the corresponding values between fine and coarse

meshes were 0.030, 0.585, and 0.057 (Fig.4), respectively. This finding reflects the fact that the free surface elevation simulated applying adaptive moving meshes was similar to that applying fixed fine meshes, especially in the local region where the free surface gradient was relatively large. However, the solution derived using the GRP scheme applying fixed coarse mesh differed significantly from adaptive moving mesh. Interestingly, the grid never appeared to be twined during the adaptive redistribution of triangular meshes from $t = 0$ to 7.2, which is an essential condition for numerical approximation of the SWEs under the adaptive moving meshes model.

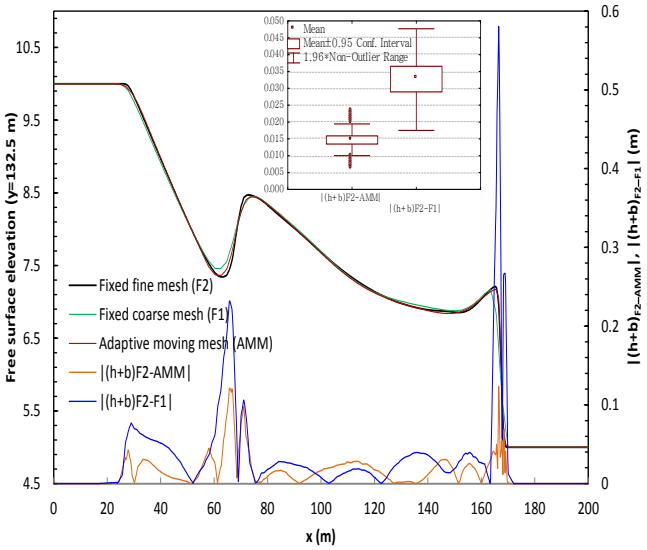


Figure 4. Comparison of the free surface elevations along the line $y = 132.5$m at $t = 7.2$ between fixed coarse, fixed fine, and adaptive moving meshes. Note: $|(h + b)\text{F2} - \text{AMM}|$ is the absolute value of the discrepancy between the numerical solutions of fixed fine and adaptive moving meshes while $|(h + b)\text{F2} - \text{F1}|$ is that between fine and coarse meshes; the Box-Whisker plot presented the mean, confident interval (0.05), and range of the discrepancies.

### *6.2. Still water flow over a smooth bed*

This test case validates the ability of the proposed scheme to satisfy the well-balanced stability-preserving property as introduced in . Bed topography is defined as:

$$B(x, y) = 0.8 \exp\left\{-50\left[(x - 0.5)^2 + (y - 0.5)^2\right]\right\}, (x, y) \in [0, 1] \times [0, 1], \tag{47}$$

the initial state was set as $h(x, y) = 1 - B(x, y)$, $u(x, y, 0) = 0$ and $v(x, y, 0) = 0$. When the triangular meshes was generated, we choose $\alpha = 50$. The initial quasi-uniform triangulation of the physical domain, as well as the logical domain, was generated with a horizontal (and vertical) boundary partition of $5,816$ cells with $3,009$ nodes. The simulation was performed until a simulation time of $t = 1.7$. Discrepancies between the exact solutions and numerical solutions using the updated GRP scheme under both fixed meshes and moving meshes ($h + b$, $u$ and $v$) were within the limits of round off error (Table II), demonstrating that the updated GRP scheme under both fixed and adaptive moving meshes exactly satisfied the well-balanced property. Compared with the numerical results ($|h + b - 1|$, $|u|$ and $|v|$) using the original GRP scheme in [15], our new numerical

schemes are significantly stable due to two-step modification for time derivative evaluation.

| Algorithm | $\|h+b-1\|$ | $\|u\|$ | $\|v\|$ |
|---|---|---|---|
| GRP scheme in [15] on fixed meshes | 1.49E-09 | 6.60E-08 | 6.43E-08 |
| updated GRP scheme on fixed meshes | 2.00E-15 | 4.06E-14 | 4.44E-14 |
| updated GRP scheme on moving meshes | 7.22E-15 | 1.39E-14 | 1.77E-14 |

Table II. Numerical solutions of GRP scheme under both fixed and moving meshes ($t = 1.7$) with $3,009$ nodes and $5,816$ cells. Note: $h + b$, $u$, and $v$ are the free surface elevation, flow velocities along $x-$ and $y-$directions, respectively; The discrepancies between the numerical and exact solutions of above current updated GRP scheme and Moving meshes scheme were within the limits of machine error while the the original GRP scheme in [15] is only 1E-08.

### *6.3. Still water with a small perturbation*

This test case validated the high-resolution predictive ability of the proposed scheme, as first introduced by [9]. The two-dimensional bottom topography consists of an elliptic hump, as follows:

$$B\left(x,y\right)=0.8\exp\left\{-5(x-0.9)^{2}+50(y-0.5)^{2}\right\},(x,y)\in[0,2]\times[0,1]\,. \tag{48}$$

The initial free surface elevation was set as:

$$h\left(x,y\right)=\begin{cases}1+\varepsilon-B\left(x,y\right), & \text{if } x\in[0.05,0.15]\,\text{m},\\ 1-B\left(x,y\right), & \text{Otherwise},\end{cases} \tag{49}$$

where $u\left(x,y,0\right)=0$ and $v\left(x,y,0\right)=0$. The free surface elevation was flat except for $0.05\leq x\leq 0.15$m, where the surface was perturbed with $\epsilon=0.01$m. Transmissive boundaries appeared on the right and left sides of the rectangular domain. In this study, we used $\alpha=20$. Model domains were divided into $14,064$ triangular cells with $8,210$ nodes for adaptive moving mesh. At $t=0$, the left propagating pulse had already left the domain because of the transmissive boundary conditions. When $t=0.12$, only the right-going portion of the disturbance was observed when it propagated over the hump (Fig. 5). Wave speed decreased above the hump due to the reduced water depth, resulting in a distortion of the initially planar perturbation.

To elucidate the high-resolution predictive capabilities, Fig. 5 shows a series of snap-shots of free surface elevation contours for shock propagation and the corresponding meshes at $t=0.12$, $0.24$, $0.36$, and $0.48$. Compared with the numerical results from previous studies [9, 49], the solutions obtained here exhibit higher-resolution shock-capturing with less meshes. The updated scheme can exactly preserve the well-balanced property and significantly improve the small-scale resolution of local features in regions with sharp flow gradient variables.

Certainly, in order to verify our updated GRP scheme, only bed slope source term was considered within SWEs system in this paper, which is same as previous works [14]. Therefore, the current proposed well-balanced scheme is only suitable for SWEs involving wet bed topography. Other source terms, such as bottom friction, wind force, Coriolis force, and viscosity force, should be partly or totally included in the SWEs to verify the capability of this scheme in field-scale applications in future work.

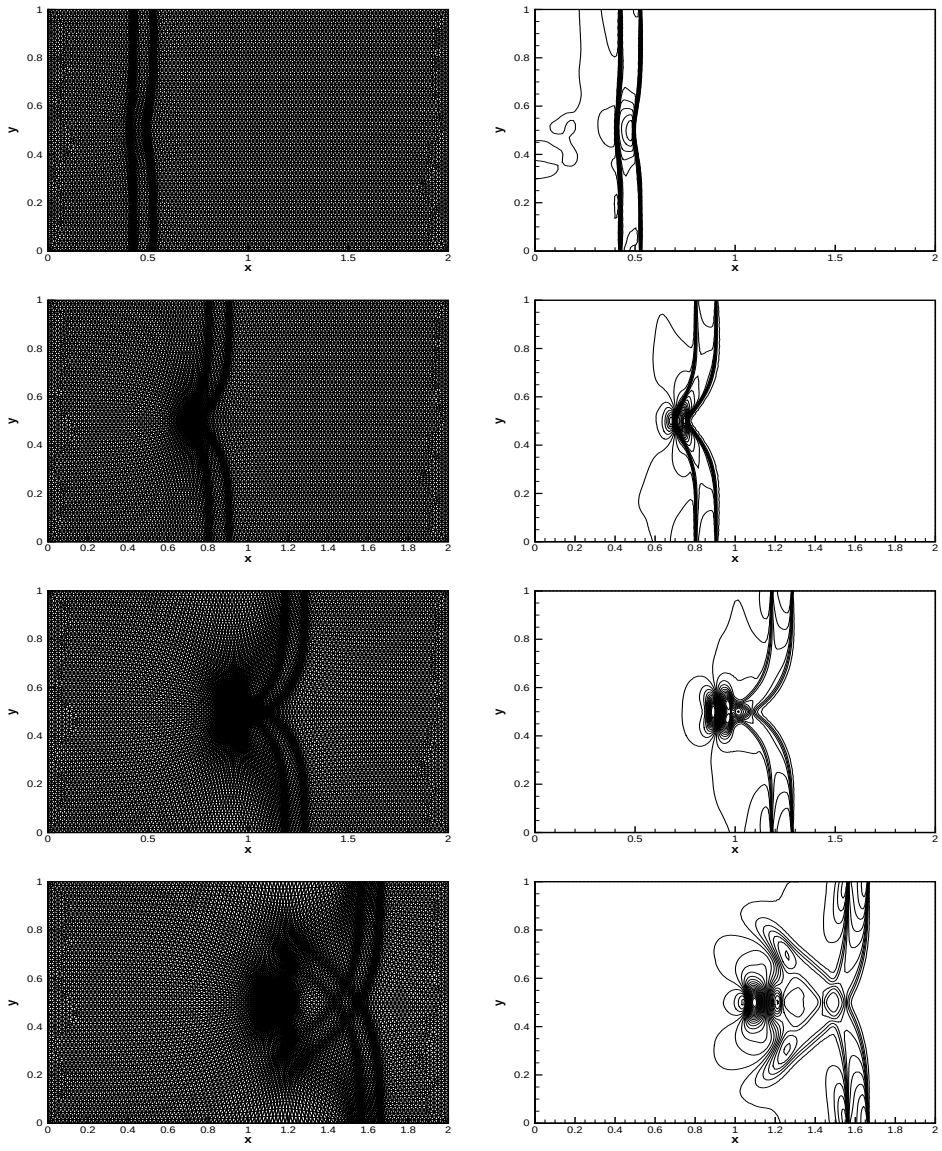

Figure 5. Numerical solutions of adaptive GRP scheme for a still water with a small perturbation. Contour lines (left side) of free surface elevation and the corresponding meshes (right side) at $t = 0.12$, $0.24$, $0.36$, and $0.48$ were illustrated.

## 7. CONCLUSIONS

This study developed a well-balanced stable GRP scheme to solve SWEs under adaptive unstructured triangular meshes, which stably and efficiently simulated the well-balanced hydrodynamic processes of shallow waters involving bed topography. Three two-dimensional examples demonstrated the shock-capturing and computational advantages of this scheme. The main features of this updated scheme can be summarized as follows:

(1) This updated scheme can solve the SWEs under triangular meshes by evaluating solutions along the exterior normal direction of the cell boundaries and by incorporating suitable central discretization of the bed source term, resulting in high-resolution simulations to balance the

bed slope and flux gradients with more stability through a modification of GRP time derivative calculation and proof of well-balance property.

(2) This scheme can dynamically approximate the gradient distribution of physical variables by iteratively solving Euler-Lagrange equations and remapping them through geometrical conservative interpolations of the free surface on new mesh with satisfaction of still flat water property; it also significantly improves the predictive ac-curacy and resolution of local features with relatively lower computational cost.

## ACKNOWLEDGEMENT

The authors wish to thank Prof. Huazhong Tang for his collaboration.

## REFERENCES

1. Audusse E, Bouchut F, Bristeau M, Klein R, Perthame B. A fast and stable well-balanced scheme with hydrostatic reconstruction for shallow water flows 2004; **25**(6):2050–2065.
2. Audusse E, Bristeau M. A well-balanced positivity preserving second-order scheme for shallow water flows on unstructured meshes 2005; **206**(1):311–333.
3. Noelle S, Pankratz N, Puppo G, Natvig J. Well-balanced finite volume schemes of arbitrary order of accuracy for shallow water flows 2006; **213**(2):474–499.
4. Lukáčová-Medvidová M, Noelle S, Kraft M. Well-balanced finite volume evolution Galerkin methods for the shallow water equations 2007; **221**(1):122–147.
5. Gallouët T, Hérard J, Seguin N. Some approximate Godunov schemes to compute shallow-water equations with topography 2003; **32**(4):479–513.
6. Jin S. A steady-state capturing method for hyperbolic systems with geometrical source terms 2001; **35**(4):631–645.
7. Jin S, Wen X. Two interface-type numerical methods for computing hyperbolic systems with geometrical source terms having concentrations 2005; **26**(6):2079–2101.
8. Kurganov A, Levy D. Central-upwind schemes for the Saint-Venant system 2002; **36**(3):397–425.
9. LeVeque R. Balancing source terms and flux gradients in high-resolution Godunov methods: the quasi-steady wave-propagation algorithm 1998; **146**(1):346–365.
10. Perthame B, Simeoni C. A kinetic scheme for the Saint-Venant system with a source term. *Calcolo* 2001; **38**(4):201–231.
11. Russo G. Central schemes for balance laws. *Hyperbolic problems: theory, numerics, applications* 2001; :821–829.
12. Ricchiuto M, Bollermann A. Stabilized residual distribution for shallow water simulations 2009; **228**(4):1071–1115.
13. Xing Y, Shu C. High order finite difference WENO schemes with the exact conservation property for the shallow water equations 2005; **208**(1):206–227.
14. Zhou J, Causon D, Mingham C, Ingram D. The surface gradient method for the treatment of source terms in the shallow-water equations 2001; **168**(1):1–25.
15. Li J, Chen G. The generalized Riemann problem method for the shallow water equations with bottom topography 2006; **65**(6):834–862.
16. Mungkasi S, Roberts S. A finite volume method for shallow water flows on triangular computational grids. *Advanced Computer Science and Information System (ICACSIS), 2011 International Conference on*, 2011; 79 – 84.
17. Xing Y, Zhang X, Shu C. Positivity-preserving high order well-balanced discontinuous Galerkin methods for the shallow water equations 2010; **33**(12):1476–1493.
18. Ben-Artzi M, Falcovitz J. *Generalized Riemann problems in computational fluid dynamics*, vol. 11. Cambridge Univ Pr, 2003.
19. Ben-Artzi M. The generalized Riemann problem for reactive flows 1989; **81**(1):70–101.
20. Ben-Artzi M, Falcovitz J. A second-order Godunov-type scheme for compressible fluid dynamics 1984; **55**(1):1–32.
21. Ta-Tsien L, Serre D, Hao Z. The generalized Riemann problem for the motion of elastic strings 1992; **23**:1189.
22. Birman A, Falcovitz J. Application of the GRP scheme to open channel flow equations 2007; **222**(1):131–154.
23. Ben-Artzi M, Li J, Warnecke G. A direct Eulerian GRP scheme for compressible fluid flows 2006; **218**(1):19–43.

24. Ben-Artzi M, Li J. Hyperbolic balance laws: Riemann invariants and the generalized Riemann problem 2007; **106**(3):369–425.
25. Bermudez A, Vazquez M. Upwind methods for hyperbolic conservation laws with source terms 1994; **23**(8):1049–1071.
26. Rosatti G, Begnudelli L. The Riemann problem for the one-dimensional, free-surface shallow water equations with a bed step: Theoretical analysis and numerical simulations 2010; **229**(3):760–787.
27. Berthon C, Foucher F. Efficient well–balanced hydrostatic upwind schemes for shallow–water equations 2012; **231**(1):49935015.
28. Brufau P, García-Navarro P, Vázquez-Cendón M. Zero mass error using unsteady wetting–drying conditions in shallow flows over dry irregular topography 2004; **45**(10):1047–1082.
29. Castro M, Ferreiro Ferreiro A, Garcia-Rodriguez J, González-Vida J, Macías J, Parés C, Elena Vázquez-Cendón M. The numerical treatment of wet/dry fronts in shallow flows: application to one-layer and two-layer systems 2005; **42**(3):419–439.
30. Gallardo J, Parés C, Castro M. On a well-balanced high-order finite volume scheme for shallow water equations with topography and dry areas 2007; **227**(1):574–601.
31. Xu K. The gas-kinetic scheme for shallow water equations. *Journal of Hydrodynamics, Ser. B* 2006; **18**(3):73–76.
32. Noelle S, Xing Y, Shu C. High-order well-balanced finite volume WENO schemes for shallow water equation with moving water 2007; **226**(1):29–58.
33. Liang Q. A simplified adaptive cartesian grid system for solving the 2d shallow water equations 2012; **69**:442458.
34. Winslow A. Numerical solution of the quasilinear poisson equation in a nonuniform triangle mesh 1966; **1**(2):149–172.
35. Ren W, Wang X. An iterative grid redistribution method for singular problems in multiple dimensions 2000; **159**(2):246–273.
36. Miller K, Miller R. Moving finite element I 1981; **18**:1019–1032.
37. Huang W, Russell R. Adaptive mesh movementthe MMPDE approach and its applications 2001; **128**(1):383–398.
38. Dvinsky A. Adaptive grid generation from harmonic maps on Riemannian manifolds 1991; **95**(2):450–476.
39. Li R, Tang T, Zhang P. Moving mesh methods in multiple dimensions based on harmonic maps 2001; **170**(2):562–588.
40. Tang H, Tang T. Adaptive mesh methods for one-and two-dimensional hyperbolic conservation laws 2003; :487–515.
41. Tang H. Solution of the shallow-water equations using an adaptive moving mesh method 2004; **44**(7):789–810.
42. Chen G, Tang H, Zhang P. Second-order accurate Godunov scheme for multicomponent flows on moving triangular meshes 2008; **34**(1):64–86.
43. Han E, Li J, Tang H. An adaptive GRP scheme for compressible fluid flows 2010; **229**(5):1448–1466.
44. Han E, Li J, Tang H. Accuracy of the Adaptive GRP scheme and the simulation of 2-d Riemann problems for compressible Euler equations 2011; **10**:577–606.
45. Han J, Tang H. An adaptive moving mesh method for two-dimensional ideal magnetohydrodynamics 2007; **220**(2):791–812.
46. Liang Q, Marche F. Numerical resolution of well-balanced shallow water equations with complex source terms 2009; **32**(6):873–884.
47. Lin G, Lai J, Guo W. Finite-volume component-wise TVD schemes for 2d shallow water equations 2003; **26**(8):861–873.
48. Namin M, Lin B, Falconer R. Modelling estuarine and coastal flows using an unstructured triangular finite volume algorithm 2004; **27**(12):1179–1197.
49. Canestrelli A, Siviglia A, Dumbser M, Toro E. Well-balanced high-order centred schemes for non-conservative hyperbolic systems. Applications to shallow water equations with fixed and mobile bed 2009; **32**(6):834–844.